Hindawi
Shock and Vibration
Volume 2021, Article ID 5514719, 11 pages
https://doi.org/10.1155/2021/5514719

Research Article

Investigation of the Scruton Number Effects of Wind-Induced Unsteady Galloping Responses of Bridge Suspenders

Shuai Zhou,[1,2,3] Yunfeng Zou,[4] Xugang Hua,[2] Fanrong Xue,[4] and Xuandong Lu[4]

[1]*China Construction Fifth Engineering Division Corp., Ltd., Zhongyi One Road No. 158, Changsha, Hunan, China*
[2]*College of Civil Engineering, Hunan University, Lushan No. 1, Changsha, Hunan, China*
[3]*China State Construction Engineering Corp., Ltd., Beijing 100013, China*
[4]*School of Civil Engineering, Central South University, Changsha 410075, Hunan, China*

Correspondence should be addressed to Yunfeng Zou; yunfengzou@csu.edu.cn

Received 1 March 2021; Accepted 6 September 2021; Published 29 September 2021

Academic Editor: Arturo Garcia-Perez

Copyright © 2021 Shuai Zhou et al. This is an open access article distributed under the Creative Commons Attribution License, which permits unrestricted use, distribution, and reproduction in any medium, provided the original work is properly cited.

When the critical wind speed of vortex-induced resonance is close to that of quasi-steady galloping, a type of coupled wind-induced vibration that is different from divergent galloping can easily occur in a rectangular bar. It is a type of "unsteady galloping" phenomenon wherein the response amplitude increases linearly with the increase in the wind speed, while a limit cycle oscillation is observed at each wind speed, whose mechanism is still in research. Mass and damping are the key parameters that affect the coupling degree and amplitude response estimation. For a set of rectangular section member models with a width-to-height ratio of 1.2, by adjusting the equivalent stiffness, equivalent mass, and damping ratio of the model system and performing comparative tests on the wind-induced vibration response of the same mass with different damping ratios, it is possible to achieve the same damping ratio with different masses and the same Scruton number with different masses and damping combinations under the same Reynolds number. The results show that the influence of the mass and damping parameters on the "unsteady galloping" amplitude response is independent, and the weight is the same in the coupling state. The Scruton number "locked interval" (12.4–30.6) can be found in the "unsteady galloping" amplitude response, and the linear slope of the dimensionless wind speed amplitude response curve does not change with the Scruton number in the "locked interval." In addition, a "transition interval" (26.8–30.6) coexists with the "locked interval" wherein the coupling state of the wind-induced vibration is converted into the uncoupled state. The empirical formula for estimating the "unsteady galloping" response amplitude is modified and can be used to predict the amplitude within the design wind speed range of similar engineering members.

1. Introduction

The classes of blunt bridge members, such as rigid bridge suspenders, whose sections are rectangular and feature large slenderness ratios, are light in mass, low in damping, and prone to the combined instability stemming from a typical vortex-induced resonance and galloping.

This unsteady galloping exhibiting some special characteristics, such as the beginning of continuous vibration at vortex resonance wind speed for rectangular cylinders, which are perpendicular to the flow, has been extensively studied by previous scholars in engineering practice research [1–4].

Coupled vibrations can even be triggered when the onset wind speeds are close to each other. The amplitude of wind-induced vibration increases with an increase in the wind speed in the coupling state. At a single wind speed point, the vibration of the bar takes the form of a "limit cycle" and "limiting amplitude" at a single wind velocity, not a typical divergent galloping response such as in iced catenary system [5]. In addition, the wind-amplitude response curve shows a linear growth trend. There is no vortex resonance locked interval and no divergent galloping at the single wind speed point. The pneumatic mechanism is unclear and has been called "unsteady galloping" by previous researchers. Sun et al. [6] studied the way to harvest the wind energy

generating from the synergetic effect of coupled vortex-induced vibration and galloping responses. While, Mohamed et al. [7] tried to suppress the coupled vibration with a downstream square plate by varying side ratios.

Niu et al. [8] established a mathematical model of "unsteady galloping" by combining the vortex excitation model of the wake oscillator with two degrees of freedom (DOF) and a quasi-stationary vibration force model. The wind speed amplitude response curve was classified according to the coupling degree. The numerical calculation results were in agreement with the results obtained by identifying the relevant aerodynamic parameters. The wind speed amplitude curve of the "unsteady galloping" response is determined by two parameters, that is, the onset wind speed U_0 of the coupled vibration and the linear slope of the wind speed amplitude response curve. The European wind resistance design code [9] suggests that a coupled vibration necessitates an onset wind speed ratio between the vortex resonance and the galloping vibration in the range of 0.7 to 1.5. The studies in [10] showed that the European code is unsafe, and the ratio should be greater than the range from 4.5 to 8.5 so that the coupled vibration can be avoided. In [11], the wind-amplitude response curve morphology of the "unsteady galloping" under different Scruton numbers was studied by adjusting the stiffness support form of the member model in the wind tunnel tests and changing the damping ratio, indicating that a Scruton number exceeding the range of 50 to 60 is a necessary condition for eliminating coupled vibration. Mannini et al. and Chen et al. [12–14] proposed a prediction model that was more consistent with the experimental results measured by modifying the aerodynamic parameters based on the 2-DOF Tamura wake oscillator model. Mannini et al. [11] investigated the influence of the wind attack angle and turbulence on the "unsteady galloping," proposing that low turbulence (approximately 3%) would enhance the coupled vibration of the vortex-induced resonance and galloping.

Niu et al. [8] proposed an empirical formula applicable to the amplitude estimation of the "unsteady galloping" of rectangular section members. Studies have shown that the linear slope of the response curve under the coupled vibration state is a function of the ratio of the width of a member section to its height (B/D). An empirical formula for amplitude estimation was proposed by accumulating a large amount of data for regression analysis. The studies in [15, 16] indicated that mass and damping are key parameters that influence the amplitude of vortex-induced resonance responses, and this influence is not independent. The degrees of influence of single parameter variations (mass or damping) on amplitude are different. Hence, the mass and damping parameters cannot be used to form the Scruton number to evaluate the amplitude response. The use of the Scruton number, as an independent parameter, was investigated in this study. The authors in [17, 18] showed that differences in the Reynolds number can result in different amplitude responses, which is also the reason behind the conclusions in [15, 16]. To evaluate the amplitude, the mass and damping parameters are usually combined as the Scruton number.

With respect to the coupled vibration between the vortex-induced resonance and galloping vibration ("unsteady galloping"), a comparative study of the parameter sensitivity of the independent mass and damping parameters, as well as the combined mass damping parameter "Scruton number," should be conducted considering the Reynolds number effect. To further study the "unsteady galloping" response mechanism and to consolidate the results of more reasonable amplitude estimation formulas, this study considers a typical rectangular section member model with a width-to-height ratio of 1.2 ($B/D = 1.2$) as a research object and adjusts the equivalent mass, equivalent stiffness, and damping ratio of the model system in order to conduct a series of wind tunnel tests on the same mass with different damping ratios, the same damping ratio with different mass values, and the same Scruton number with different mass and damping combinations. It also measures and draws the curve of the wind speed amplitude responses to comparatively study the influence of the mass and damping parameters.

2. Theoretical Model

2.1. Wake Oscillator Model. A diagram of the cylinder flow wake oscillator is shown in Figure 1. The cylinder tail following the cylinder flow can form a nearly stable vortex that oscillates up and down and provides an oscillator that can interact with the vibration of the cylinder. The oscillator mass is formed by the air quality, and the fluid-solid coupled shear stiffness of the vortex oscillating up and down is the vibrator stiffness. It can be simplified as a vortex-induced force mechanics model with a 2-DOF wake oscillator, as shown in Figure 2. In the figures, U is the incoming flow wind speed, D is the diameter of the cylinder, L is the half width of the wake vortex, H is the height of the wake vortex, G is the center of gravity of the wake vortex still air, and α is the angular displacement of the up-and-down oscillation of the wake oscillator. Furthermore, I, K, and C are the torsional mass, torsional stiffness, and aerodynamic damping of the wake oscillator, respectively. The vibration equation of the established Birkhoff model is given by

$$I \cdot \frac{\mathrm{d}^2\alpha}{\mathrm{d}t^2} + C \cdot \frac{\mathrm{d}\alpha}{\mathrm{d}t} + K \cdot \alpha = 0. \tag{1}$$

For a two-dimensional (2D) cylinder, Tamura considered the influence of changes in the wake vibrator length in the vibration period. He also proposed a modified Birkhoff 2-DOF vortex-induced resonance mathematical model:

$$\begin{aligned} &\ddot{\alpha} - 2\zeta\nu\left\{1 - \left(\frac{4f^2}{C_{L0}^2}\right)\alpha^2\right\}\dot{\alpha} + \nu\alpha = -m^*\ddot{Y} - \nu S^*\dot{Y}, \\ &\ddot{Y} + \left\{2\eta + \frac{n(f + C_D)\nu}{S^*}\right\}\dot{Y} + Y = -\frac{fm\nu^2\alpha}{S^{*2}}, \\ &C_L = -f\left(\frac{\alpha + S^*\dot{Y}}{\nu}\right), \end{aligned} \tag{2}$$

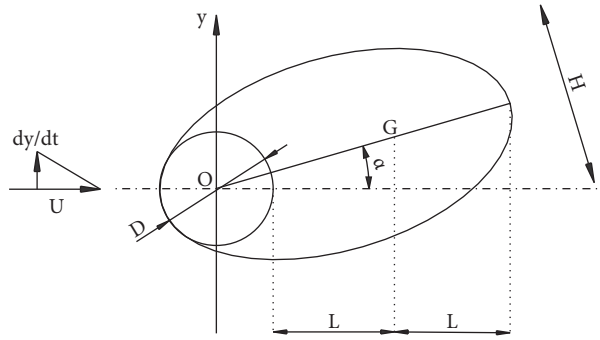

Figure 1: Diagram of the wake oscillator.

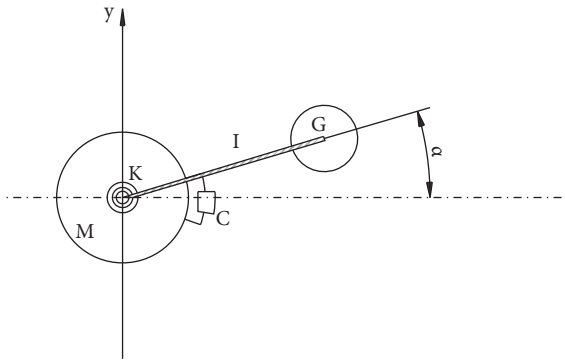

Figure 2: Mechanical model of the wake oscillator.

where Y is the dimensionless displacement response of the structure, α is the displacement response of the wake oscillator, n is the mass ratio, η is the mechanical damping ratio of the structure, ν is the dimensionless fluid velocity, C_D is the cylinder resistance coefficient, f is the Magnus effect aerodynamic parameter, Hr is the dimensionless wake oscillator width, and C_{L0} is the lift coefficient amplitude of a cylinder at rest [19, 20].

According to the quasi-constant galloping force theory, the aerodynamic force can be obtained, as shown in equation (3). The research conclusion in [8] shows that the expansion term of the Taylor series for the quasi-constant galloping force can essentially meet the calculation requirements with consideration of the seventh order, and equation (4) is defined as the coefficient of the quasi-constant galloping force:

$$F_y = -\frac{1}{2}\rho U^2 D \cdot \left[A_1 \cdot \left(\frac{\dot{y}}{U}\right) + A_2 \cdot \left(\frac{\dot{y}}{U}\right)^2 + A_3 \cdot \left(\frac{\dot{y}}{U}\right)^3 + A_4 \cdot \left(\frac{\dot{y}}{U}\right)^4 + A_5 \cdot \left(\frac{\dot{y}}{U}\right)^5 + \Delta\left(\frac{\dot{y}}{U}\right)^n\right], \tag{3}$$

$$C_{FY} = A_1 \cdot \left(\frac{\dot{y}}{U}\right) + A_2 \cdot \left(\frac{\dot{y}}{U}\right)^2 + A_3 \cdot \left(\frac{\dot{y}}{U}\right)^3 + A_4 \cdot \left(\frac{\dot{y}}{U}\right)^4 + A_5 \cdot \left(\frac{\dot{y}}{U}\right)^5 + \Delta\left(\frac{\dot{y}}{U}\right)^n. \tag{4}$$

As shown in equation (5), the dynamic model of the vortex-induced resonance and galloping aerodynamic coupling is formed by combining the quasi-stationary galloping self-excited force model with the vortex-induced force mechanics model and the 2-DOF wake oscillator proposed by Tamura:

$$\begin{aligned}
&\ddot{\alpha} - 2\zeta\nu\left\{1 - \left(\frac{4f^2}{C_{L_0}^2}\right)\alpha^2\right\}\dot{\alpha} + \nu\alpha = -m^*\ddot{Y} - \nu S^*\dot{Y},\\
&\ddot{Y} + \left\{2\eta + \frac{n(f - A_1)\nu}{S^*} - \frac{nA_2S^*}{\nu\dot{Y}} - nA_3\left(\frac{S^*}{\nu}\right)^3\dot{Y}^2 - \cdots\right\}\dot{Y} + Y = -\frac{fn\nu^2\alpha}{S^{*2}},\\
&C_L = -\left\{(f - A_1)\frac{S^*\dot{Y}}{\nu} - A_2\left(\frac{S^*\dot{Y}}{\nu}\right)^2 - A_3\left(\frac{S^*\dot{Y}}{\nu}\right)^3 - \cdots + f\alpha\right\},
\end{aligned} \tag{5}$$

where A_1, A_2, A_3, ... are the polynomial coefficients of the Taylor series expansion of the quasi-constant galloping force, and the meanings of the other symbols are the same as mentioned above. The coupling model can qualitatively predict the vortex-induced resonance and galloping and identify the complete separation of the vortex-induced resonance locked interval, divergent galloping, and coupling "unsteady galloping" response, according to the degree of similarity between the two onset wind speeds. The identification, such as the recognition accuracy of the onset wind speed point of the dimensionless speed-amplitude response curve and amplitude response, depends on the accuracy of the related aerodynamic parameters. It should be pointed out that there is no analytical but numerical solution for equation (5), and the numerical solution could be obtained by the Runge–Kutta mathematical method through numerical iteration.

For the coupled vortex-induced vibration and galloping phenomenon, based on the previous classical 2-DOF wake oscillator model, Mannini [21] proposed a more useful model by taking into account the effects of turbulence intensity and integral length scale and verified by wind tunnel tests. Gao et al. [22] proposed an empirical model by considering the aerodynamic nonlinearity with two amplitude-dependent damping terms and aerodynamic unsteadiness by expressing aerodynamic parameters as functions of reduced frequency. Chen et al. [23] investigated the unsteady effects from field measurement wake-induced vibrations of aligned hangers of long-span suspension bridge.

2.2. Classification of "Unsteady Galloping" Response Curves. According to the degree of coupling between the vortex-induced resonance and galloping, the wind-amplitude response curve of the "unsteady galloping" can be divided into two types, that is, the coupling state and the uncoupled state. From the study in [19], the response curves measured when the onset wind speed ratios of the galloping and vortex-induced resonance were 1.06, 1.49, and 2.15 are shown in Figure 3. The working conditions (a) and (b) are under the "coupling state." The amplitude increases as the wind speed gradually increases. The features of the vortex-induced resonance in the "locked interval" do not appear in the response curve. The time history of the amplitude curve at a single wind speed indicates a stable state with a constant amplitude, and divergent galloping does not appear. The amplitude linearly increases with an increase in the wind speed. The features of the response curve can be described by calculating the slope of the curve. The ratio of the onset wind speed between the galloping and vortex-induced resonance further increases to 2.15, and the working condition (c) shows the "uncoupled state." With the increase in the wind speed, the separated "locked interval" of the limiting vortex-induced resonance and the galloping response appear in the amplitude response curve.

3. Wind Tunnel Test

3.1. Model and Setting. All tests were performed in a closed-circuit wind tunnel at the Hunan University, China. The

Figure 3: Installation of the sectional model in the wind tunnel.

cross sections of the test section had a width of 3.0 m, height of 2.5 m, and maximum wind velocity of up to 58 m/s. All the tests were designed to be performed under smooth flow conditions. The model size of the rectangular member section for the wind tunnel test is 100 mm × 120 mm × 1530 mm, and the ratio of the section width to its height is $B/D = 1.2$. The installation of the model in the wind tunnel test is shown in Figure 3. The model stiffness is provided by eight vertical mounting springs, and the system stiffness can be adjusted by changing the springs. The mass of the system is composed of the mass of the section model itself, the end plate, the connecting rod, the weight of the spring reduction, and the balance weight. The equivalent mass of the model system can be adjusted by increasing or decreasing the balance weight. The natural damping of the model system can be effectively increased by wrapping tape around the spring. The damping of the system can be identified before and after the wind tunnel experiments for the model vibration measurement. The comparison results show that the damping is essentially the same, which indicates that the damping is stable after the model system undergoes substantial wind-induced vibrations.

Acceleration sensors are used in the wind tunnel tests to measure vibrations. The installation diagram is shown in Figure 4. A total of four acceleration sensors (#1, #2, #3, and #5) with a sampling frequency of 500 Hz were placed at the front and rear above the horizontal connecting rod at both ends of the section model on its windward and leeward sides. The section model system has six possible degrees-of-freedom (DOFs), as shown in Figure 5. There are three translational DOFs and three rotational DOFs along with *X*-*X*, *Y*-*Y*, and *Z*-*Z* axes, respectively. The translational DOFs in the directions of the *X*-*X* and *Z*-*Z* axes were restricted in the section modal system, as well as the rotational DOF in the direction of the *Y*-*Y* axis. The other three available DOFs of the section model system were the translational DOFs in the directions of the *Y*-*Y* axis (heaving mode) and *Z*-*Z* axis (rolling mode), respectively, as well as the rotational DOF in the direction of the *X*-*X* axis (pitching mode). The recognition of the vibration form and processing of the amplitude response can be performed via signal processing using the four acceleration sensors. Through the adjustment of the torsional rigidity of the section model system, the vibration modes, with the exception of the heaving mode, are

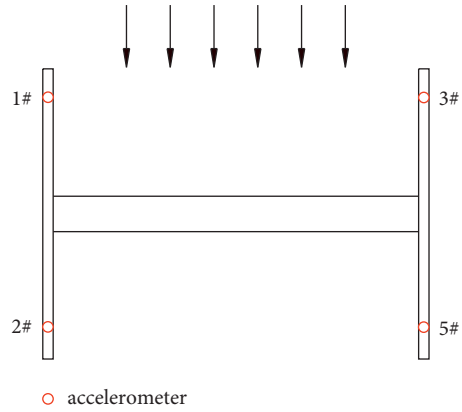

Figure 4: Indication of a sensor installation on the sectional model.

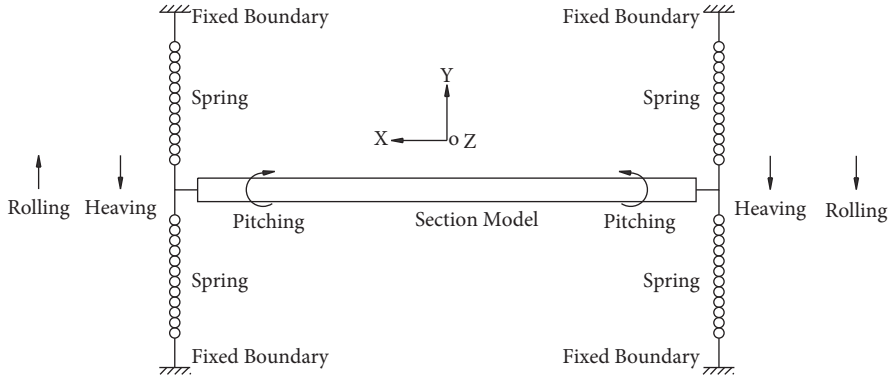

Figure 5: Potential vibration mode of the sectional model.

eliminated in all working conditions studied herein; the ratio of the torsional frequency to the vertical frequency is from 3.5–4.5. The vibration acceleration response of the section model was obtained by determining the weighted average of the time-history signals of the four sensors. According to the features of the simple harmonic single-frequency vibration, displacement response signals can be easily obtained using acceleration vibration signals.

3.2. Configurations and Parameters. A comparison of the main parameters of the three-dimensional (3D) prototype prism with those of the 1 : 1 2D section model is presented in Table 1. The surface roughness of the prototype prism and section model differ. The steel prototype prism was painted as smoothly as possible to make it similar to the organic glass material section model. Both the 3D prototype prism and the 2D section model have the same cross-sectional dimensions and roughly the same mass, damping, and natural frequencies. The Reynolds number corresponds to the peak of the VIV lock-in.

The physical quality per linear meter of the section model system is divided into four different levels using counterweights: 8.27 kg/m, 10.53 kg/m, 11.73 kg/m, and 16.08 kg/m. The equivalent damping of the vertical bending is divided into five different levels through the combination of quality and damping parameters *A*1–*A*20: 0.146%, 0.200%, 0.223%, 0.284%, and 0.500%. A total of 20 test working configurations were established by combining the mass and damping parameters. The wind-induced vibration responses under the combinations of working configurations, such as "the same mass with different damping ratios" and "the same damping ratio with different masses," can be comparatively studied.

The Scruton number ranges from 12.4 to 82.5. When the Scruton number is 24.1, the wind-induced vibration response can be observed under the configuration that has the same Scruton number with a combination of different mass and damping parameters. By co-adjusting the equivalent mass and equivalent stiffness of the model system, the bending natural frequencies in the vertical direction of *A*1–*A*20 are consistent, and the Reynolds number of the onset wind speed corresponding to the vortex-induced resonance is the same. The effect generated by the Reynolds number is eliminated to study the influence of the mass and damping parameters on the "unsteady galloping" response.

4. Results and Discussion

4.1. Coupling State. The time-history curve of the typical wind-induced vibration was obtained by conducting an experiment with a rectangular section member model (*A*1

Table 1: Working configurations of research and parameters.

Case number	m (kg/m)	ξ (%)	Scruton	Spring stiffness (N/m)	Measured frequency (Hz)	Reynolds	V_g/V_v
A1		0.284	24.1				2.8
A2		0.223	18.9				2.2
A3	8.27	0.200	17.0	616	2.93	16000	2.0
A4		0.146	12.4				1.5
A17		0.500	42.5				5.0
A5		0.223	24.1				2.8
A6		0.284	30.6				3.6
A7	10.53	0.200	21.6	767	2.93	16000	2.5
A8		0.146	15.8				1.9
A18		0.500	54.0				6.4
A9		0.200	24.1				2.8
A10		0.284	34.1				4.0
A11	11.73	0.223	26.8	852	2.93	16000	3.2
A12		0.146	17.6				2.1
A19		0.500	60.2				7.1
A13		0.146	24.1				2.8
A14		0.284	46.8				5.5
A15	16.08	0.223	36.8	1181	2.93	16000	4.3
A16		0.200	33.0				3.9
A20		0.500	82.5				9.7

Note. $Sc = 4\pi M\xi/\rho D^2$ is the Scruton number, M is the equivalent mass of the structural damping ratio, ρ is the air density, D is the model upwind height, V_g is the galloping onset wind speed, V_v is the primary wind speed of the vortex-induced resonance, and ξ is damping ratio, identified from decaying curves of acceleration. The Reynolds number corresponds to the onset wind speed point of the vortex-induced resonance vibration.

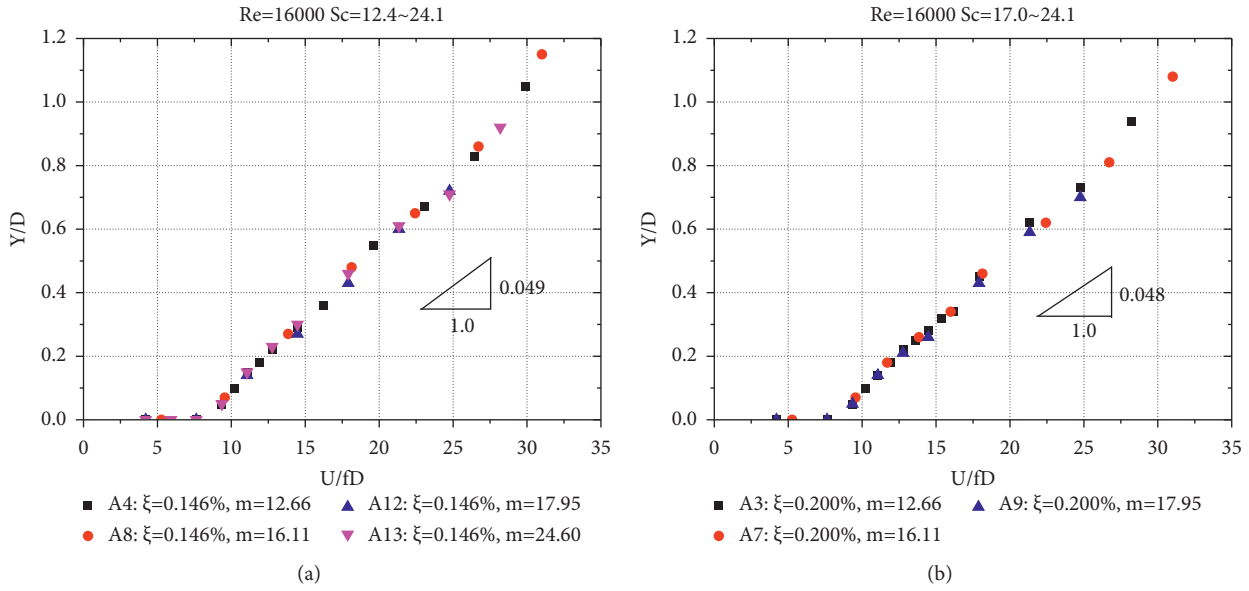

Figure 6: Comparison of different quality responses. (a) $\xi = 0.146\%$. (b) $\xi = 0.200\%$.

working configuration, flow velocity $U = 3.7$ m/s), as shown in Figure 6. Under the action of stable wind speed, the model is essentially in a state of constant amplitude vibration, with a small-amplitude "beat frequency phenomenon." Four acceleration sensors were installed at the front, rear, windward, and leeward sides of the sectional model. They measured the time-history curve with the same phase, which indicated that the vibration of the model had no torsion or swaying mode and was completely a vertical vibration. An analysis of the Fourier transformation (FFT) spectrum corresponding to the measured time-history curve is shown in Figure 7. The remarkable vibration frequency is 2.93 Hz, which is consistent with the measured natural frequency in the vertical direction under the static wind state and is a single-frequency vibration state.

By adjusting and matching the equivalent mass and equivalent stiffness of the model system, the natural frequency of the vertical vibration under the static wind state of

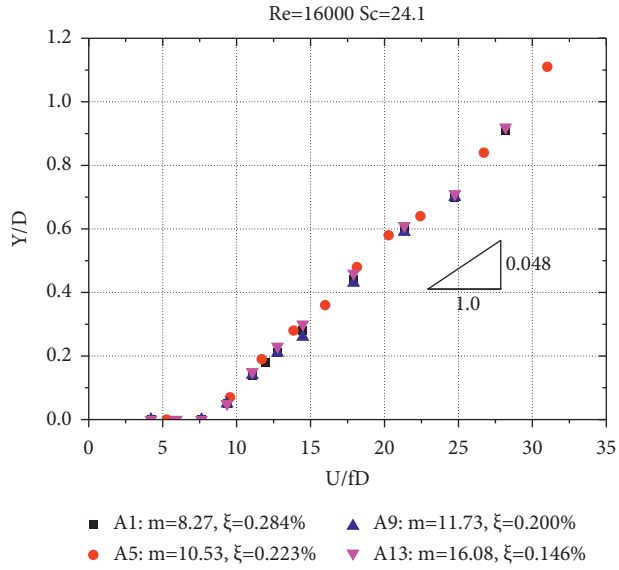

Figure 7: Comparison of different quality and damping responses (Sc = 24.1).

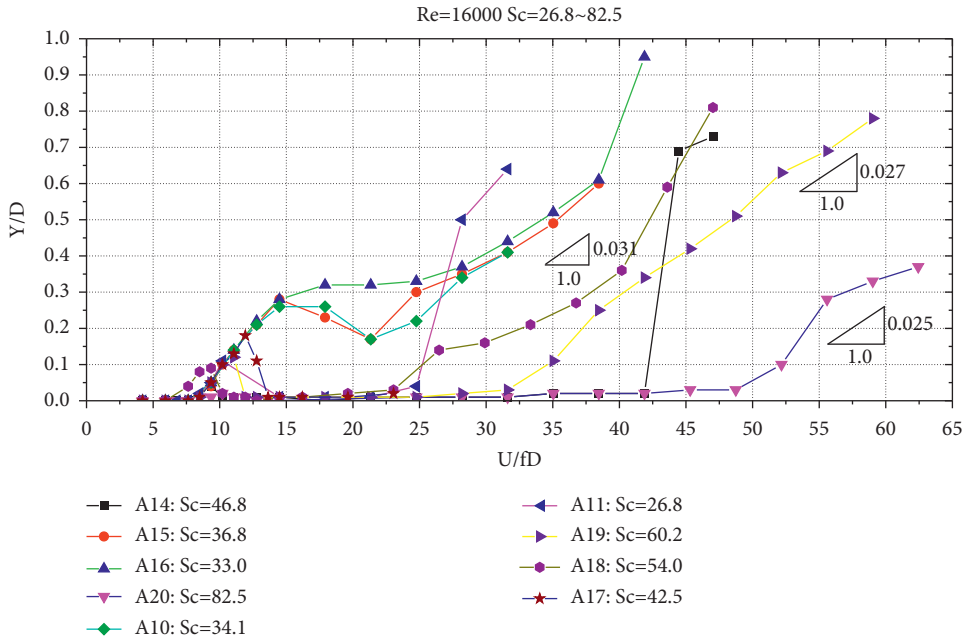

Figure 8: Amplitude response under dimensionless wind speed in the uncoupled state.

the configuration $A1$–$A20$ in all the working configurations studied herein is the same, that is, 2.93 Hz. This corresponds to the Reynolds number Re = 16000 of the onset wind speed of the vortex-induced resonance. The same mass $m = 8.27$ kg/m is used in the $A1$, $A2$, $A3$, and $A4$ working configurations with different damping ratios of $\xi = 0.146\%$, 0.200%, 0.223%, and 0.284%. The curves of the dimensionless wind-amplitude response corresponding to the Scruton numbers ranging from 12.4 to 24.1 are shown in Figure 8. In the figure, the dimensionless wind speed is defined as U/fD, where U is the incoming flow wind speed, $F = 2.93$ Hz is the outstanding vibration frequency, and $D = 100$ mm is the windward height of the rectangular member. The dimensionless amplitude is Y/D, where Y is the displacement amplitude response. According to the simple harmonic features of the single-frequency vibration in the time-history curve, as shown in Figure 1, the amplitude of the displacement responses is obtained based on the acceleration signal.

It can be seen from Figure 9(a) that the curves of the dimensionless wind-amplitude responses in the configurations $A1$ to $A4$ basically coexist. The dimensionless onset wind speed is 7.5, and the corresponding Strouhal number is 0.13, which is higher than the value

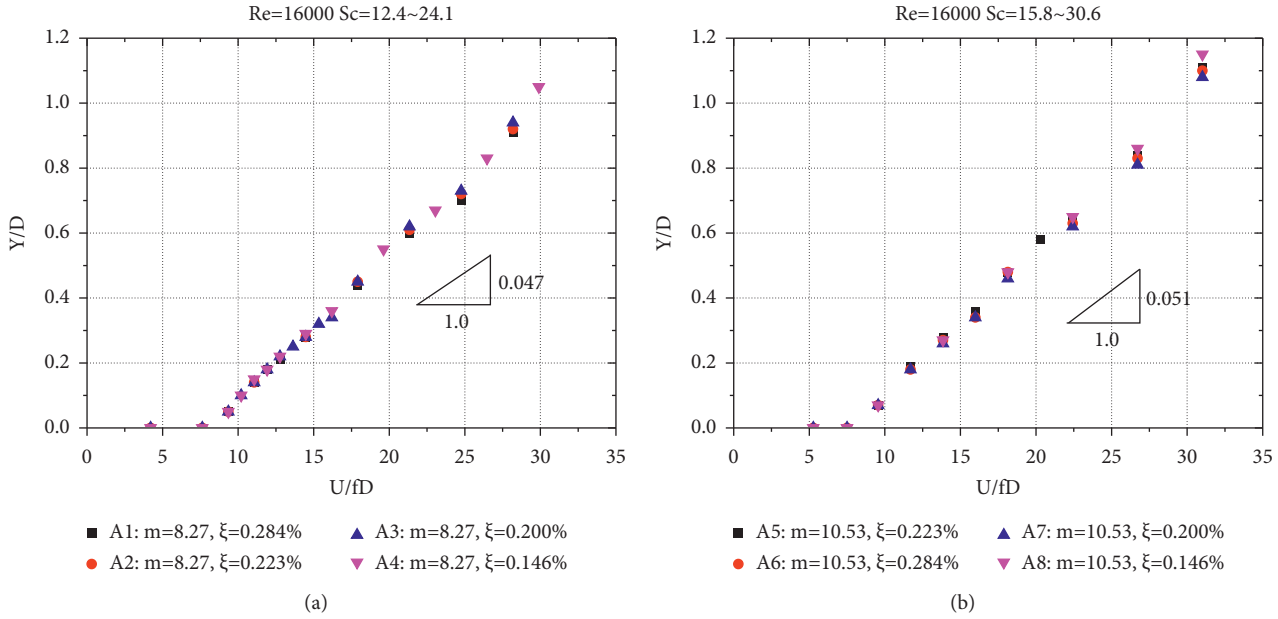

Figure 9: Comparison of different damping responses. (a) $m = 8.27$ kg/m. (b) $m = 10.53$ kg/m.

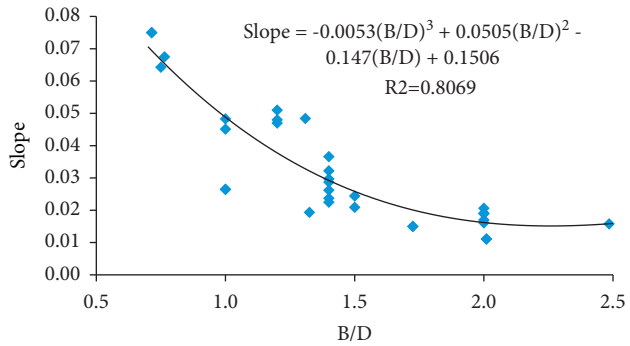

Figure 10: Fitting of response slope value and ratio of width to height of rectangular section.

recommended by the European specifications. The curve of the dimensionless wind-amplitude responses shows a linear growth trend, and the slope value is 0.047 after the start of the vibration. Figure 9(b) shows the corresponding working configurations *A*5, *A*6, *A*7, and *A*8 with an equivalent mass of $m = 10.53$ kg/m. The combinations of different damping ratios of 0.146%, 0.200%, 0.223%, and 0.284% correspond to the curve of the dimensionless wind-amplitude responses with Scruton numbers ranging from 15.8 to 30.6. The response trend and features are consistent with those in Figure 8(a), in which the obtained slope value is 0.051. It can be seen from the comparison results that, under the same mass parameter, the damping ratio of the studied rectangular section with a width-to-height ratio of 1.2 changes from 0.146% to 0.284%, which has no influence on the trend of vibration responses and the slope value of "unsteady galloping." The variation range of the corresponding Scruton number is from 12.4 to 30.6.

Figure 6(a) shows a comparison of the vibration responses through experiments on the measured models in wind tunnel tests under the combined configuration "same damping ratio and different masses." The measured damping ratios of configurations *A*4, *A*8, *A*12, and *A*13 are 0.146% with equivalent masses of $m = 12.66$ kg/m, 16.11 kg/m, 17.95 kg/m, and 24.60 kg/m, respectively. These correspond to the curves of the dimensionless wind-amplitude responses of the Scruton numbers ranging from 12.4 to 24.1. The response curves of the four working configurations tend to coincide. The vibration point of the dimensionless wind speed was 7.5 and the slope value was 0.049. As shown in Figure 10, the damping ratio of 0.200% and equivalent mass $m = 12.66$ kg/m, 16.11 kg/m, and 17.95 kg/m in the working configurations *A*3, *A*7, and *A*9 are essentially the same as those in Figure 6(b). The slope value of the dimensionless response curve was 0.048. It can be seen from the comparison of the test results that the equivalent mass of the model system changes from 12.66 kg/m to 24.60 kg/m at the same damping level and the Scruton number ranges from 12.4 to 24.1. The obtained curve of the dimensionless wind-amplitude responses has the same onset wind speed point. Furthermore, the slope of the amplitude response after vibration is the same.

Figure 7 shows a comparison of the curve of the dimensionless wind speed amplitude responses with different combinations of mass and damping when the Scruton number (24.1) is the same. The dimensionless wind speed obtained at the starting point is 7.5 and the slope value of the curve after vibration is 0.048. The response curve features do not change with the different combinations of mass and damping parameters, as shown in Figures 8 and 10. The study shows that when the width-to-height ratio is 1.2 of the rectangular member section model with a Scruton number ranging from 12.4 to 30.6, the coupling of the vortex-

induced resonance and galloping produces an "unsteady galloping" response. The response curves obtained by conducting experiments on different working configurations, such as the same mass with different damping ratios, the same damping ratio with different masses, and the same Scruton number with different combinations of mass and damping ratio, are essentially the same. The onset wind speed point of the curves of the dimensionless displacement amplitude responses is 7.5, corresponding to a Strouhal number of 0.13. The linear slopes of the curves of the amplitude responses are essentially the same, with a small amplitude range of 0.047–0.051.

It can be speculated that there exists a Scruton number "locked interval" for the "unsteady galloping" response, which behaved under similar phenomenon as vortex-induced vibration lock-in. In the "locked interval," the response curve of the wind speed amplitude does neither change with the change in the value of the single mass and damping parameter nor with the change in the overall Scruton number. The onset wind speed point and slope value of the amplitude curve are always locked at the same value. For the bar studied herein, the "locked interval" is 12.4–30.6.

4.2. Uncoupled State. Figure 8 shows a comparison of the curve of the dimensionless wind speed amplitude responses under the uncoupled state of the vortex-induced resonance and galloping in the working configurations from $A1$ to $A20$ listed in Table 1. The response curve of the uncoupled state mainly takes on three forms: the locked interval and large-amplitude galloping response of the complete-separation vortex-induced resonance, the locked interval and large-amplitude galloping response of the semiseparation vortex-induced resonance, and the locked interval and large-amplitude galloping response of the negligible vortex-induced resonance.

The studies in [10, 11] show that the critical wind speed ratio of the galloping and vortex-induced resonance is in the interval 4.5–8.5, and a Scruton number ranging from 50 to 60 is a necessary condition to avoid the occurrence of coupled vibration. The present study shows that the vortex-induced resonance can be separated from galloping to produce uncoupled vibrations if the critical wind speed ratio between the galloping and the vortex-induced resonance ranges from 3.2 to 9.7, corresponding to the Scruton number from 26.8 to 82.5. In the states of complete separation and semiseparation, the galloping response can be divided into two types: divergent vibration and limit cycle limited vibration at a single wind speed point. Among them, the slope values of 0.025–0.031 of the galloping response dimensionless wind amplitude obtained under the action of high wind speed ($U/fD > 15$) in the limit cycle vibration state are significantly lower than those in the coupling state of 0.047–0.051. This is possibly attributable to the disappearance of the coupled action, resulting in a lack of the contribution of the vortex-induced aerodynamic force in the state of limit cycle vibration. Accordingly, this weakens the energy accumulation and decreases the amplitude response.

It is worth noting that the Scruton number corresponding to the "unsteady galloping" response of the coupling state in the experimentally studied condition is 12.4–30.6, and it is 26.8–82.5 in the uncoupled state. There is an overlapping interval of the Scruton number (26.8–30.6), which can be considered the "transition interval" of the Scruton number from the coupling state to the uncoupled state.

4.3. Modified Empirical Formula for Amplitude Estimation. With regard to the fact that the onset wind speed of the "unsteady galloping" response can be roughly determined by the Strouhal law and the fact that the dimensionless response amplitude increases linearly with the dimensionless wind speed after vibration, Niu et al. [8] identify two key parameters, that is, the onset wind speed point U_0 and the linear growth slope. A numerical study and regression analysis were then carried out, and an empirical formula for amplitude estimation was presented. The research shows that the slope of the key parameters of the empirical formula is a function of the ratio of the width to the height (B/D) of the rectangular section bar, and the relevant mathematical expressions are obtained through polynomial fitting based on a large amount of measured data.

Based on the measured "soft vibration" response data of the rectangular section bar in the wind tunnel test with a width-to-height ratio (B/D) of 1.2, the regression analysis database of the original empirical formula is supplemented based on previous work [8], and a modified empirical formula for amplitude estimation is proposed through polynomial fitting:

$$\frac{Y}{D} = \left(-0.0053 \cdot \left(\frac{B}{D}\right)^3 + 0.0505 \cdot \left(\frac{B}{D}\right)^2 - 0.147 \cdot \frac{B}{D} + 0.1506\right) \cdot (U_r - U_0), \tag{6}$$

where Y/D is the dimensionless wind speed, $U_r = U/(fD)$ is the dimensionless incoming wind speed, $U_0 = 0.9/\mathrm{St}$ is the onset wind speed point of the "unsteady galloping" based on the Strouhal number normalization of the section, and B/D is the width-to-height ratio of the rectangular section. It should be noted that the empirical formula is applicable only in coupled vortex-induced vibration and galloping cases.

It should be pointed out that the error of the empirical formula is a little large due to limited collected data, the measured origin data is scattered which can be observed in Figure 10, and the deviation is supposed to be contracted as data collected more densely in the future work.

5. Conclusions

(1) For the present rectangular suspender whose aspect ratio is 1.2, the vibration response is unrelated to the mass and damping parameters under the coupling state.

(2) There is a Scruton number "locked interval" which makes the "unsteady galloping" response curves'

slope have no relation to the changes of single mass, damping, and combined Scruton number. The "locked interval" of the present rectangular suspender is 12.4–30.6.

(3) The onset wind speed ratio of the vortex-induced resonance and galloping is determined by the Scruton number. The magnitude of the ratio determines the coupling degree of the "unsteady galloping." The results show that there is a Scruton number "transition interval," which causes the model vibration to transition from the coupling state to the uncoupled state. For present rectangular suspender, it is 26.8–30.6.

(4) A modified empirical formula for amplitude estimation of "unsteady galloping" is proposed, and it can provide a reference for relevant engineering designs.

Data Availability

The data used to support the findings of this study are available from the corresponding author upon request.

Conflicts of Interest

The authors declare that there are no conflicts of interest regarding the publication of this paper.

Acknowledgments

The authors gratefully acknowledge the support of the National Natural Science Foundations of China (Project nos. 51708202, 52078504, and 51422806), Scientific Research Plan of Hunan Province of China (Project no. 2019RS2051), Innovation-Driven Project of Central South University (no. 2020CX009), and Scientific Research Plan of China State Construction Engineering Group (Project no. CSCEC-2020-Z-43).

References

[1] T. Andrianne, R. P. Aryoputro, P. Laurent, and G. Colson, "Energy harvesting from different aeroelastic instabilities of a square cylinder," *Journal of Wind Engineering and Industrial Aerodynamics*, vol. 172, pp. 164–169, 2018.

[2] S. Cammelli, A. Bagnara, and J. G. Navarro, "VIV-galloping interaction of the deck of a footbridge with solid parapets," *Procedia Engineering*, vol. 199, pp. 1290–1295, 2017.

[3] G. Gao and L. Zhu, "Measurement and verification of unsteady galloping force on a rectangular 2:1 cylinder," *Journal of Wind Engineering and Industrial Aerodynamics*, vol. 157, pp. 76–94, 2016.

[4] F. Petrini and K. Gkoumas, "Piezoelectric energy harvesting from vortex shedding and galloping induced vibrations inside HVAC ducts," *Energy and Buildings*, vol. 158, pp. 371–383, 2018.

[5] G. Chen, Y. Yang, Y. Yang, and Li Peng, "Study on galloping oscillation of iced catenary system under cross winds," *Shock and Vibration*, vol. 2017, no. 2, pp. 1–16, Article ID 1634292, 2017.

[6] W. Sun, S. Jo, and J. Seok, "Development of the optimal bluff body for wind energy harvesting using the synergetic effect of coupled vortex induced vibration and galloping phenomena," *International Journal of Mechanical Sciences*, vol. 156, pp. 435–445, 2019.

[7] A. Mohamed, S. A. Zaki, M. Shirakashi, M. S. Mat Ali, and M. Z. Samsudin, "Experimental investigation on vortex-induced vibration and galloping of rectangular cylinders of varying side ratios with a downstream square plate," *Journal of Wind Engineering and Industrial Aerodynamics*, vol. 211, Article ID 104563, 2021.

[8] H. Niu, S. Zhou, Z. Chen, and X. Hua, "An empirical model for amplitude prediction on VIV-galloping instability of rectangular cylinders," *Wind and Structures*, vol. 21, no. 1, pp. 85–103, 2015.

[9] EN1991-1-4 Eurocode 1-actions on Structures, *Parts 1–4*, General Actions-Wind Actions, London, UK, 2010.

[10] C. Mannini, A. M. Marra, and G. Bartoli, "VIV-galloping instability of rectangular cylinders: review and new experiments," *Journal of Wind Engineering and Industrial Aerodynamics*, vol. 132, pp. 109–124, 2014.

[11] C. Mannini, A. M. Marra, T. Massai, and G. Bartoli, "VIV and galloping interaction for a 3:2 rectangular cylinder," in *Proceedings of the Sixth European and African Conference on Wind Engineering*, Cambridge, UK, July 2013.

[12] C. Mannini, A. M. Marra, T. Massai, and G. Bartoli, "Interference of vortex-induced vibration and transverse galloping for a rectangular cylinder," *Journal of Fluids and Structures*, vol. 66, pp. 403–423, 2016.

[13] C. Mannini, T. Massai, and A. M. Marra, "Modeling the interference of vortex-induced vibration and galloping for a slender rectangular prism," *Journal of Sound and Vibration*, vol. 419, pp. 493–509, 2018.

[14] Z. Chen, K. T. Tse, K. C. S. Kwok, A. Kareem, and B. Kim, "Measurement of unsteady aerodynamic force on a galloping prism in a turbulent flow: a hybrid aeroelastic-pressure balance," *Journal of Fluids and Structures*, vol. 102, Article ID 103232, 2021.

[15] Z. Chen, Y. Xu, H. Huang, and K. T. Tse, "Wind tunnel measurement systems for unsteady aerodynamic forces on bluff bodies: review and new perspective," *Sensors*, vol. 20, no. 16, p. 4633, 2020.

[16] T. Sarpkaya, "Hydrodynamic damping, flow-induced oscillations, and biharmonic response," *Journal of Offshore Mechanics and Arctic Engineering*, vol. 117, no. 4, pp. 232–238, 1995.

[17] R. N. Govardhan and C. H. K. Williamson, "Defining the "modified Griffin plot" in vortex-induced vibration: revealing the effect of Reynolds number using controlled damping," *Journal of Fluid Mechanics*, vol. 561, pp. 147–180, 2006.

[18] S. Kumar and S. Sen, "Transition of VIV-only motion of a square cylinder to combined VIV and galloping at low Reynolds numbers," *Ocean Engineering*, vol. 187, no. 3, Article ID 106208, 2019.

[19] Y. Tamura and G. Matsui, "Wake-oscillator model of vortex-induced oscillation of circular cylinder," *Journal of Wind Engineering and Industrial Aerodynamics*, vol. 1981, pp. 13–24, 1981.

[20] Y. Tamura and A. Amano, "Mathematical model for vortex-induced oscillations of continuous systems with circular cross section," *Journal of Wind Engineering and Industrial Aerodynamics*, vol. 14, no. 1-3, pp. 431–442, 1983.

[21] C. Mannini, "Incorporation of turbulence in a nonlinear wake-oscillator model for the prediction of unsteady galloping

response," *Journal of Wind Engineering and Industrial Aerodynamics*, vol. 200, Article ID 104141, 2020.

[22] G. Gao, L. Zhu, J. Li, and W. Han, "Modelling nonlinear aerodynamic damping during transverse aerodynamic instabilities for slender rectangular prisms with typical side ratios," *Journal of Wind Engineering and Industrial Aerodynamics*, vol. 197, Article ID 104064, 2020.

[23] W.-L. Chen, W.-H. Yang, F. Xu, and C.-G. Zhang, "Complex wake-induced vibration of aligned hangers behind tower of long-span suspension bridge," *Journal of Fluids and Structures*, vol. 92, Article ID 102829, 2020.